Supplementary Information (SI) for Materials Chemistry Frontiers.

Electronic Supplementary Information for

Converting coal gasification slags into monolithic supercapacitor electrodes via endogenous Fe-catalyzed growth of N-doped carbon nanotubes

Zhengguo Zhang*[a,b], Mengjuan Xu,[a,b] Fang Wang[a,b] and Shixiong Min*[a,b,c]

[a] *School of Chemistry and Chemical Engineering, North Minzu University, Yinchuan, 750021, P. R. China.*

[b] *Ningxia Key Laboratory of Solar Chemical Conversion Technology, North Minzu University, Yinchuan, 750021, P. R. China.*

[c] *Analysis and Testing Center of Ningxia Hui Autonomous Region, North Minzu University, Yinchuan, 750021, P. R. China.*

*Corresponding author: zhangzhengguo1119@126.com; sxmin@nun.edu.cn

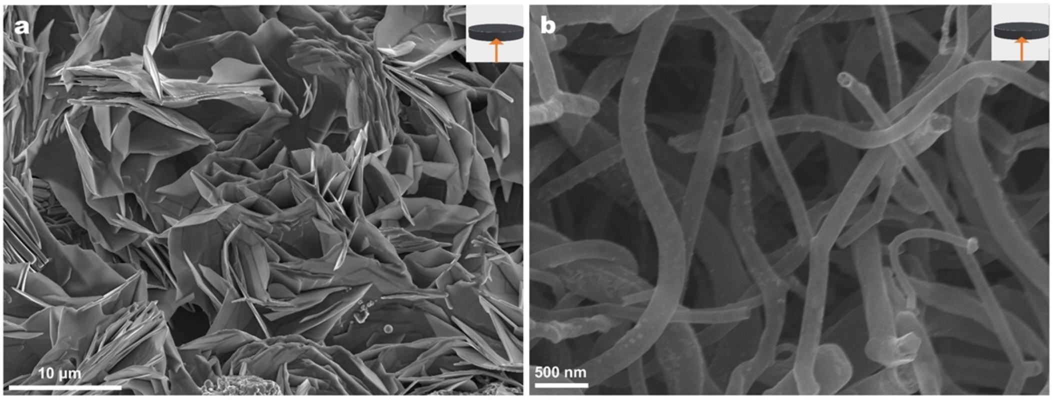

Fig. S1 Side-view SEM images of (a) S-CGS and (b) Fe_3C@NCNTs/CGS monolithic electrode.

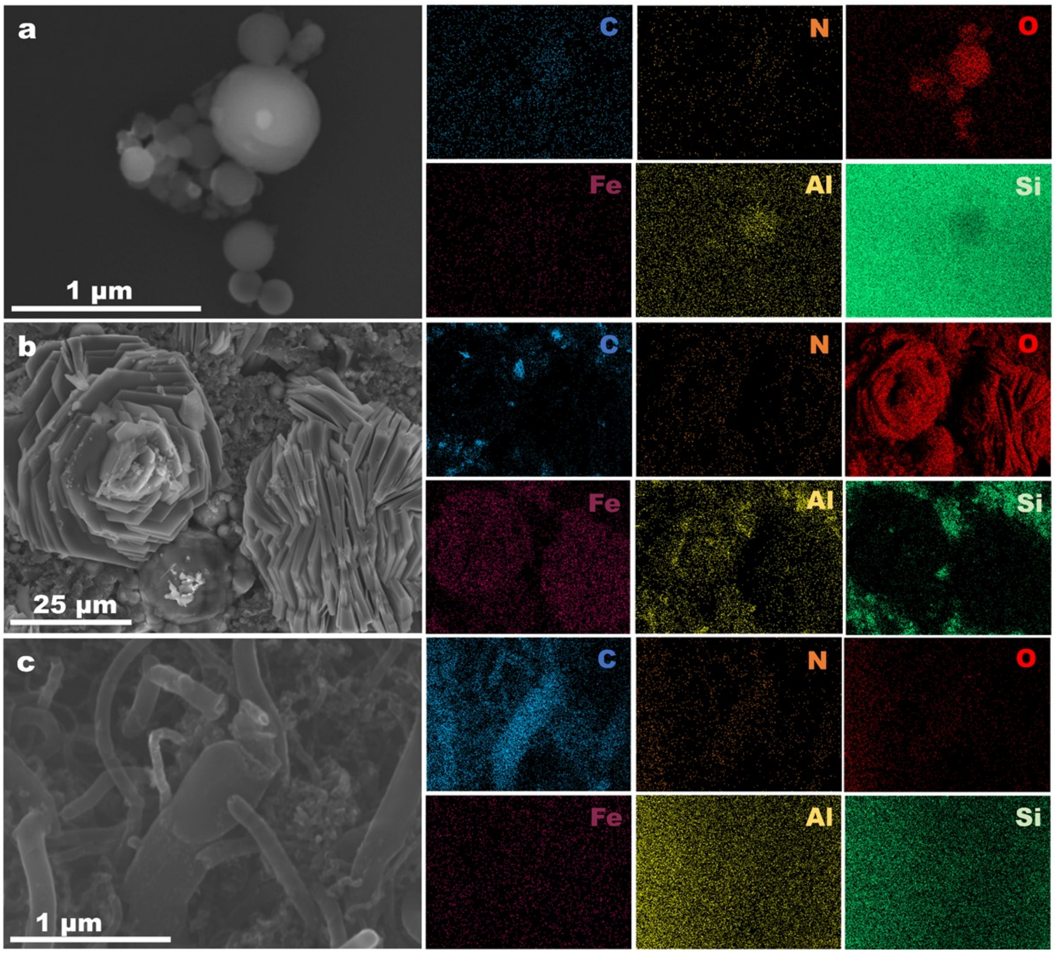

Fig. S2 SEM image of the (a) CGS, (b) S-CGS, and (c) Fe_3C@NCNTs/CGS monolithic electrode and the corresponding EDX elemental maps (C, N, O, Fe, Al, and Si).

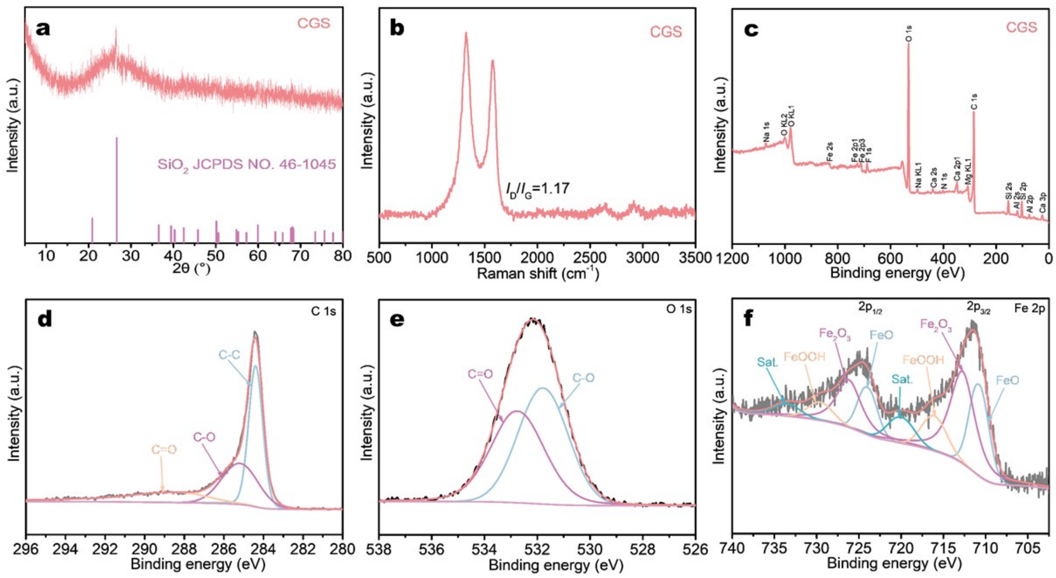

Fig. S3 (a) XRD pattern and (b) Raman spectra of CGS. (c) XPS survey spectrum and high-resolution (d) C 1s, (e) O 1s, and (f) Fe 2p XPS spectra of CGS.

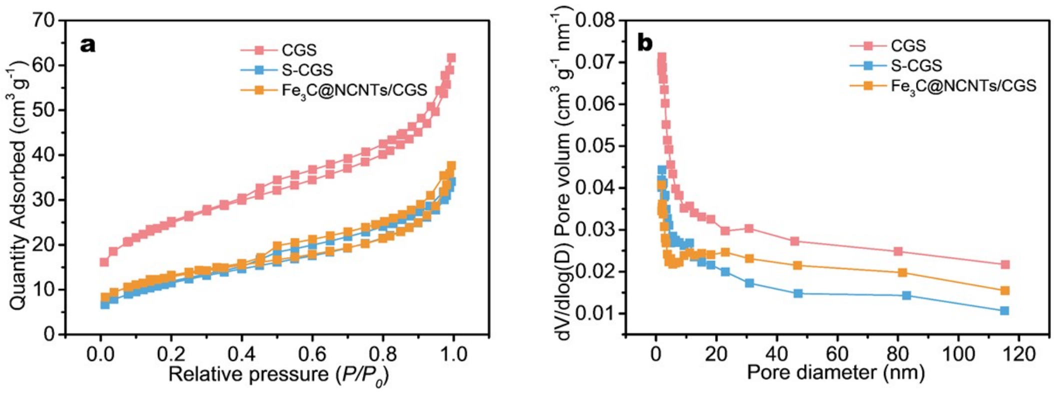

Fig. S4 (a) N_2 adsorption-desorption isotherms and (b) pore size distributions of CGS, S-CGS, and Fe_3C@NCNTs/CGS monolithic electrode.

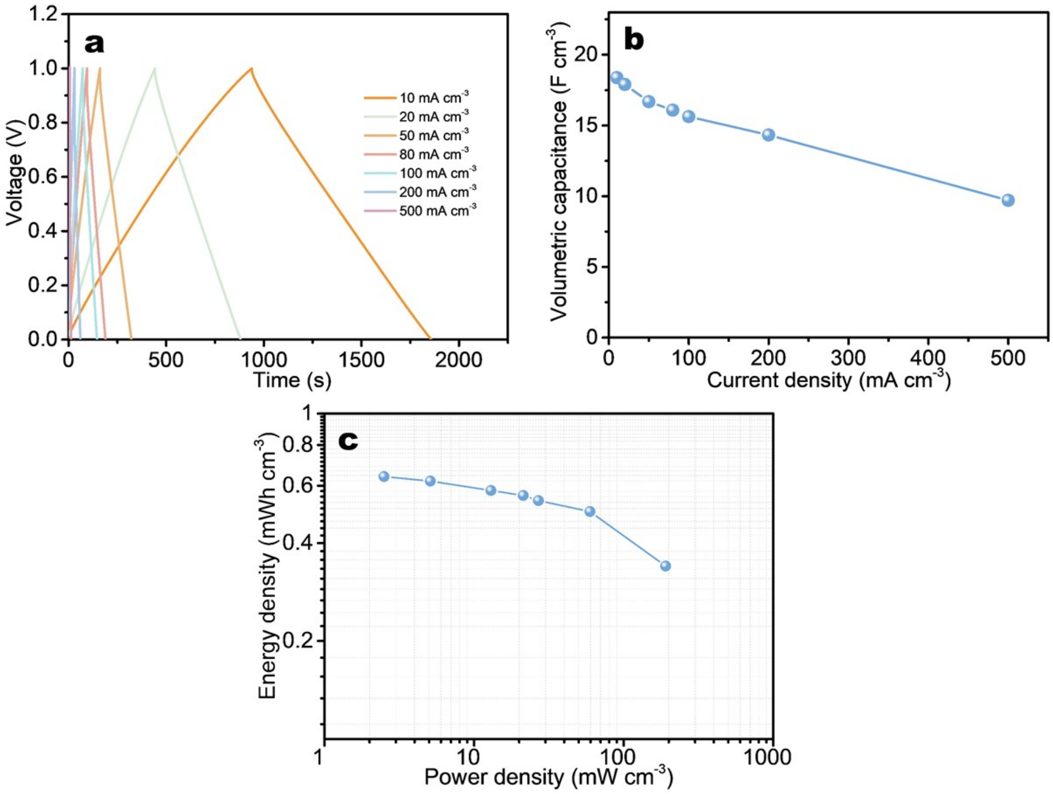

Fig. S5 (a) GCD curves of the Fe_3C@NCNTs/CGS-based SC at different current densities. (b) The volumetric capacitances of the Fe_3C@NCNTs/CGS-based SC at different current densities. (c) Ragone plot of Fe_3C@NCNTs/CGS-based SC.

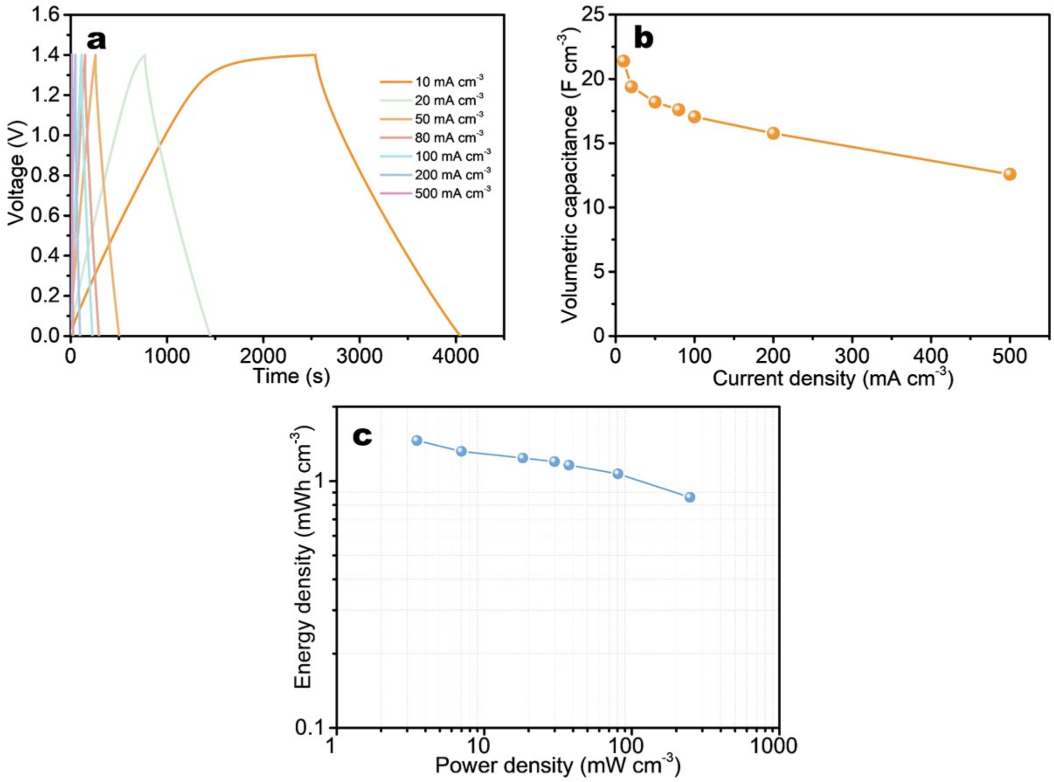

Fig. S6 (a) GCD curves of the Fe_3C@NCNTs/CGS-based SC at different current densities. (b) The volumetric capacitances of the Fe_3C@NCNTs/CGS-based SC at different current densities. (c) Ragone plot of Fe_3C@NCNTs/CGS-based SC.

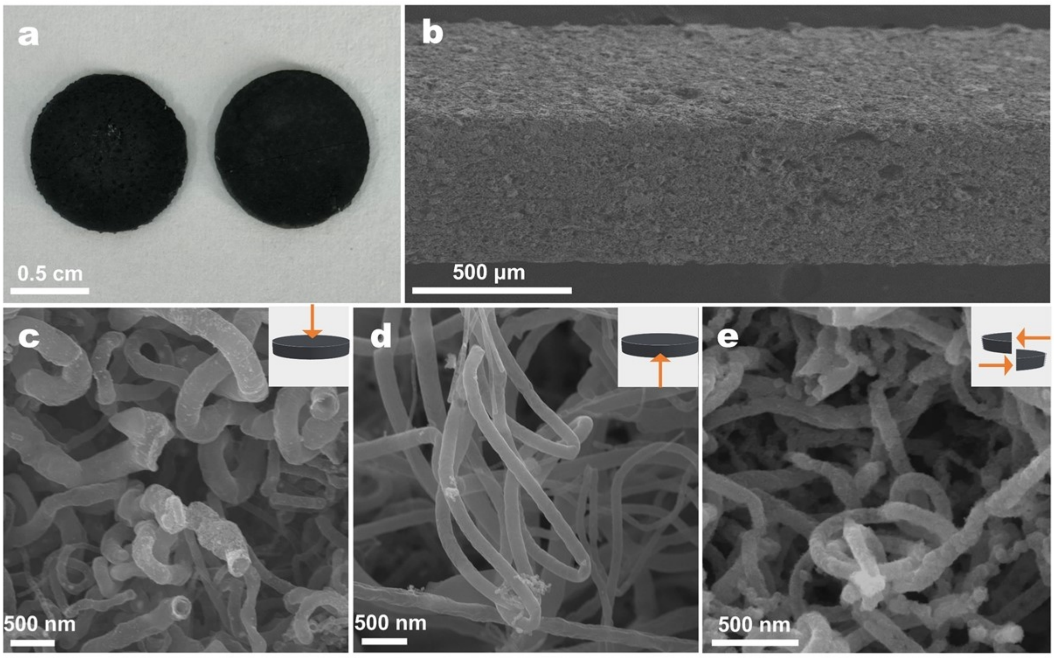

Fig. S7 (a) Digital photograph of the Fe_3C@NCNTs/CGS monolithic electrode after the cycling stability test. (b) SEM image showing the overall view of the used Fe_3C@NCNTs/CGS electrode. (c) Top-view, (d) side-view, and (e) cross-sectional view SEM images of the used Fe_3C@NCNTs/CGS electrode.

Table S1 Comparison of electrochemical performance of the Fe_3C@NCNTs/CGS electrode with reported carbon-based electrodes.

Electrode	Electrolyte	C_a (F cm^{-2})	Cycling stability	Ref.
SN-NiCo-LDH@CNTs@NCF	1.0 M KOH	4.94 C cm^{-2} (5 mA cm^{-2})	91% (5000 cycles)	1
PO-PC	1.0 M TEATFB/PC	144.14 F g^{-1} (0.1 A g^{-1})	95.61 % (1000 cycles)	2
MWCNTs/$Co_3Fe_4(PO_4)_6$	0.5 M KOH	3688 F g^{-1} (5 mV s^{-1})	98 % (5000 cycles)	3
A-NOCNS	2 M KOH	276.35 F g^{-1} (0.5 A g^{-1})	90.23 % (20000 cycles)	4
B-(NiO@$SWNT_{10}$)	2 M KOH	1257.7 F g^{-1} (1 A g^{-1})	98.3 % (10000 cycles)	5
$N_{0.5}$AC-2.3V-5h	6 M KOH	274 F g^{-1} (0.1 A g^{-1})	87.7 % (5000 cycles)	6
$PCNS_{20-1073}$	6 M KOH	296.2 F g^{-1} (0.05 A g^{-1})	97.2 % (11000 cycles)	7
AMC800	6 M KOH	282 F g^{-1} (0.5 A g^{-1})	93.45 % (10000 cycles)	8
AC-K-P	6 M KOH	212 F g^{-1} (0.1 A g^{-1})	97.52 % (2500 cycles)	9
NMCs	6 M KOH	205 F g^{-1} (0.5 A g^{-1})	100 % (10000 cycles)	10
CNT/NF	6 M KOH	737.4 mFcm^{-2} (1 mA cm^{-2})	96.41 % (10000 cycles)	11
MnO_2/CNTs	0.5 M Na_2SO_4	3310 mF cm^{-2} (1 mA cm^{-2})	78.81 % (10000 cycles)	12
CNT/prGO/PANi	1.0 M H_2SO_4	706 mF cm^{-2} (0.1 mA cm^{-2})	78% (3000 cycles)	13
CC/CNT/CuS/FeOOH	1 M KOH	1956.1 mFcm^{-2} (1 mA cm^{-2})	97.4% (500 cycles)	14
CGCM@GNS&CNT	1.5 M Na_2SO_4	441 mF cm^{-2} (1 mA cm^{-2})	102.5 % (2000 cycles)	15
Mn-MOFs/CNTs/CC	1.0 M KOH	385.8 mF cm^{-2} (0.8 mA cm^{-2})	118 % (5000 cycles)	16
Fe_3@NCNTs/CGS	6 M KOH	1955.93 mF cm^{-2} (1 mA cm^{-2})	105.23% (50000 cycles)	This work

References

1 L. Song, X. H. Zhong, F. L. Wang, Z. H. Huang, Z. Hong, Y. F. Gao, H. D. Wang, J. W. Ren, S. J. Peng, L. Li, Convenient room-temperature synthesis of sulfur and nitrogen co-doped NiCo-LDH coupled with CNTs on NiCo foam as battery-type electrode for high performance hybrid supercapacitor, *Rare Met.*, 2024, **43**, 4286-4301.

2 Zhang Z, Xiao J, Zhong Q. Structural evolution of porous carbon heteroatom doping under oxidant on supercapacitor performance, *Mater Today Chem.*, 2023, **29**, 101416.

3 T. B. Deshmukh, A. C. Mendhe, C. Padwal, D. Dubal, D. Y. Kim, B. R. Sankapal, Unlocking the synergetic potential of cobalt iron phosphate and multiwalled carbon nanotube composites towards supercapacitor application, *J. Mater. Chem. A*, 2024, **12**, 9896-9908.

4 Y. Han, C. Y. Zhang, K. J. Chen, T. Wang, 2D metal-organic framework derived ultra-thin nitrogen-doped oxygen rich porous carbon nanosheets for zinc-ion hybrid supercapacitors, *J. Mater. Chem. A*, 2024, **12**, 24296-24307.

5 X. J. Hao, W. Q. Zhou, Z. Huang, Y. Z. Li, D. Q. Li, J. K. Xu, High-performance soft-packaged supercapacitors with high energy density enabled by advanced boron-modified single-walled carbon nanotubes-enhanced nickel oxide, *J. Colloid Interface Sci.*, 2025, **689**, 137200.

6 Y. Mao, H. W. Xie, X. Chen, Y. Zhao, J. K. Qu, Q. S. Song, Z. Q. Ning, P. F. Xing, H. Y. Yin, A combined leaching and electrochemical activation approach to converting coal to capacitive carbon in molten carbonates, *J. Clean. Prod.*, 2020, **248**, 119218.

7 He XJ, Ma H, Wang JX, Xie YY, Xiao N, Qiu JS. Porous carbon nanosheets from coal tar for high-performance supercapacitors. *J Power Sources.*, 2017,

357, 41.

8 Liu YH, Qu XX, Huang GX, Xing BL, Fan YF, Zhang CX, Cao YJ. Microporous carbon derived from anthracite as supercapacitor electrodes with commercial level mass loading. *J Energy Storage.*, 2021, **43**, 103200.

9 Ma WP, Xiao RL, Wang XX, Lv XL, Zhang WF, Wang WJ, Li YP, Li MF, Hou LY, Gong Y, Zhang Y, Chen CM. Chemical co-activated modified small mesoporous carbon derived from nature anthracite toward enhanced supercapacitive behaviors. *J Electroanal Chem.*, 2022, **917**, 116417.

10 Sun F, Gao JH, Yang YQ, Zhu YW, Wang LJ, Pi XX, Liu X, Qu ZB, Wu SH, Qin YK. One-step ammonia activation of zhundong coal generating nitrogen-doped microporous carbon for gas adsorption and energy storage. *Carbon.*, 2016, **109**, 747.

11 S.-H. Kao, K. S. Anuratha, S.-Y. Wei, J.-Y. Lin, C.-K. Hsieh, Facile and Rapid Electrochemical Conversion of Ni into $Ni(OH)_2$ Thin Film as the Catalyst for Direct Growth of Carbon Nanotubes on Ni Foam for Supercapacitors, *NANOMATERIALS-BASEL*, 2022, **12**, 3867.

12 J.-H. Liu, J.-L. Yang, F. Yang, J. Feng, X.-Y. Yuan, J. Zhou, X.-J. Ma, W.-B. Zhang, A renewable bifunctional structural supercapacitor using the recycled geopolymer membrane and MnO_2/CNTs electrode, *J. Energy Storage*, 2024, **102**, 114203.

13 M. Jiang, Y. Chen, Z. Lin, Y. Zhao, L. Hou, Polyaniline enhanced partially reduced graphene oxide/carbon nanotube composite films as free-standing electrodes for flexible solid-state supercapacitors, *Diamond Relat. Mater.*, 2025, **154**, 112106.

14 Y. Zhang, D. Wang, H. Niu, H. Chen, L. Yang, L. Bai, Y. Liang, D. Wei, H.

Yang, Construction of CNT/CuS/FeOOH hierarchical composites on carbon cloth for high-performance solid-state flexible supercapacitors, *Electrochim. Acta*, 2023, **469**, 143256.

15 W. He, P.-G. Ren, Z. Dai, X. Hou, F. Ren, Y.-L. Jin, Hierarchical porous carbon composite constructed with 1-D CNT and 2-D GNS anchored on 3-D carbon skeleton from spent coffee grounds for supercapacitor, *Appl. Surf. Sci.*, 2021, **558**, 149899.

16 S. Lu, F. Xie, H. Liu, Y. Liu, Z. Zhang, W. Shang, J. Jiang, Y. Wen, Construction and electrochemical properties of carbon nanotube composite Mn-MOFs materials electrode for high-performance flexible supercapacitors, *Electrochim. Acta*, 2023, **466**, 143063.